

# Unsupervised Learning for Joint Beamforming Design in RIS-aided ISAC Systems

Junjie Ye, *Student Member, IEEE*, Lei Huang, *Senior Member, IEEE*, Zhen Chen, *Senior Member, IEEE*, Peichang Zhang, Mohamed Rihan, *Senior Member, IEEE*

**Abstract**—It is critical to design efficient beamforming in reconfigurable intelligent surface (RIS)-aided integrated sensing and communication (ISAC) systems for enhancing spectrum utilization. However, conventional methods often have limitations, either incurring high computational complexity due to iterative algorithms or sacrificing performance when using heuristic methods. To achieve both low complexity and high spectrum efficiency, an unsupervised learning-based beamforming design is proposed in this work. We tailor image-shaped channel samples and develop an ISAC beamforming neural network (IBF-Net) model for beamforming. By leveraging unsupervised learning, the loss function incorporates key performance metrics like sensing and communication channel correlation and sensing channel gain, eliminating the need of labeling. Simulations show that the proposed method achieves competitive performance compared to benchmarks while significantly reduces computational complexity.

**Index Terms**—Integrated sensing and communication, reconfigurable intelligent surface, beamforming design, unsupervised learning.

## I. INTRODUCTION

RECONFIGURABLE intelligent surface (RIS) and integrated sensing and communication (ISAC) are two promising technologies that empower future communication networks. ISAC facilitates the coexistence of sensing and communication systems within the same spectrum, while RIS enables channel adjustments to enhance spectrum efficiency [1] [2]. To fully leverage their potentials, numerous research endeavors have explored RIS-aided ISAC systems. In [3], the authors employed the semi-definite relaxation (SDR) and majorization-minimization (MM) to maximize radar signal-to-noise ratio (SNR). Similarly, a successive lower-bound maximization approach was proposed for beamforming design in a comparable scenario in [4]. Moreover, [5] considered maximizing radar signal-to-interference-plus-noise ratio (SINR) under various communication constraints. Despite exhibiting superior performance, these methods entail high computational complexities due to iterations. In contrast, a heuristic non-iterative method introduced in [6], designed RIS phases through subspace rotation and obtained the transmitter with a closed-form expression. Albeit the non-iterative method is time

efficient, its solution is obtained via direct gradient descent, rendering it susceptible to sub-optimality.

Concurrently, deep learning (DL) has attracted significant attentions due to its ability to efficiently address highly non-convex problems. Therefore, numerous studies explored DL-aided beamforming design. In [7], a fully-connected network (FCN) was utilized to predict RIS beamformers, trained offline through supervised learning. Conversely, in [8] and [9], unsupervised learning was employed to train RIS beamforming networks, thereby without the need for extensive labeling. Similarly, a lightweight unsupervised network was proposed for RIS phase design in [10]. Reinforcement learning (RL) was employed to optimize RIS phases in [11]. Beyond RIS beamformer design, DL also aids in ISAC beamforming. In [12], a FCN was trained to predict tracking beams, while [13] introduced unsupervised learning to manage interference in ISAC systems. In [14], RL was leveraged for ISAC beamformer design to allocate resource. However, these endeavors primarily focused on either RIS or ISAC beamformer design.

Against the above background, we propose an unsupervised DL approach for beamforming design in a RIS-aided ISAC system, aiming to simultaneously reduce complexities and ensure adequate system performance. Our method entails image-shaped channel samples design and the development of an ISAC beamforming neural network (IBF-Net). To mitigate labeling overhead, we devise a loss function based on unsupervised learning, considering equilibrium between sensing and communication channel correlation, along with sensing channel gain. Through simulations, we validate the efficacy of our approach, demonstrating its ability to expedite beamforming design and reduce performance degradation. The code is available online (<https://github.com/Yejacky456/DL-Beamforming-RIS-ISAC>).

## II. SYSTEM MODEL AND FORMULATIONS

We consider a RIS-aided ISAC system, where a  $M$ -antenna ISAC base station (BS) is deployed to simultaneously sense a target and serve a single-antenna user. The RIS has  $N$  passive elements to adjust the channel environment. Specifically, BS transmits ISAC signal  $\mathbf{w}_s$ , where  $s$  is the original baseband signal with unit power and  $\mathbf{w} \in \mathbb{C}^{M \times 1}$  denotes the transmit beamformer. The transmit signal propagates through channel  $\mathbf{G} \in \mathbb{C}^{N \times M}$  from BS to RIS. After tuning phases at RIS, the signal propagates through the channel  $\mathbf{h}_{r,c}^H \in \mathbb{C}^{1 \times N}$  to the user while illuminates the target through channel  $\mathbf{h}_{r,t}^H \in \mathbb{C}^{1 \times N}$ . With the target illuminated, the echo signal is reflected at RIS and

J. Ye, L. Huang, Z. Chen and P. Zhang with the State Key Laboratory of Radio Frequency Heterogeneous Integration, Shenzhen University, Shenzhen 518060, China; M. Rihan is with the Faculty of Electronic Engineering, Menoufia University, Menouf, Menoufia, Egypt (e-mail: 2152432003@email.szu.edu.cn; lhuang@szu.edu.cn; chenz.scut@gmail.com; pzhang@szu.edu.cn; mohamed.elmelegy@eleng.menoufia.edu.eg). (Corresponding author: Lei Huang.)

received by the BS. Consequently, the signal received by the user is given as

$$y_c = \mathbf{h}_{r,c}^H \Theta^H \mathbf{G} \mathbf{w} s + n_c, \quad (1)$$

in which  $\Theta = \text{diag}(e^{j\tilde{\theta}_1}, e^{j\tilde{\theta}_2}, \dots, e^{j\tilde{\theta}_N}) \in \mathbb{C}^{N \times N}$  represents the matrix of phase shifts, wherein the diagonal elements correspond to the phase shifts of each RIS element, denoted by  $\tilde{\theta}_i$ . The term  $n_c$  represents the noise at the user, assumed to adhere to additive white Gaussian noise (AWGN) with a distribution of  $\mathcal{CN}(0, \sigma_c^2)$ . Utilizing the reception model delineated in (1), the SNR at the user can be mathematically expressed as

$$\gamma_c = \frac{|\mathbf{h}_c^H \mathbf{w}|^2}{\sigma_c^2}, \quad (2)$$

where  $\mathbf{h}_c^H = \mathbf{h}_{r,c}^H \Theta^H \mathbf{G}$  represents the end-to-end communication channel. Alternatively,  $\mathbf{h}_c^H$  is also given as  $\mathbf{h}_c^H = \mathbf{v}^H \Phi_c$ , in which  $\Phi_c = \text{diag}(\mathbf{h}_{r,c}^H) \mathbf{G} \in \mathbb{C}^{N \times M}$  denotes the cascaded channel towards the user, and  $\mathbf{v} = \text{diag}(\Theta) \in \mathbb{C}^{N \times 1}$ .

Similarly, the target echo received by the BS is given as

$$\mathbf{y}_r = \mathbf{G}^H \Theta \mathbf{h}_{r,t} \mathbf{h}_{r,t}^H \Theta^H \mathbf{G} \mathbf{w} s + \mathbf{n}_r, \quad (3)$$

where  $\mathbf{n}_r \in \mathbb{C}^{N \times 1}$  represents the AWGN at BS with a distribution of  $\mathcal{CN}(0, \sigma_r^2 \mathbf{I}_M)$ . The echo SNR is then given as

$$\gamma_r = \frac{\|\mathbf{H}_t \mathbf{w}\|^2}{\sigma_r^2}, \quad (4)$$

wherein  $\mathbf{H}_t = \mathbf{h}_t \mathbf{h}_t^H$  and  $\mathbf{h}_t^H = \mathbf{h}_{r,t}^H \Theta^H \mathbf{G}$ . Also,  $\mathbf{h}_t^H$  can be reformulated as  $\mathbf{v}^H \Phi_t$ , where  $\Phi_t = \text{diag}(\mathbf{h}_{r,t}^H) \mathbf{G} \in \mathbb{C}^{N \times M}$ .

In this scenario, we aim to maximize the sensing SNR of the echo signal by jointly optimizing transmit beamformer  $\mathbf{w}$  and RIS phase shift matrix  $\Theta$ . The corresponding optimization problem can be formulated as

$$\max_{\mathbf{w}, \Theta} \gamma_r \quad (5a)$$

$$s.t. \quad \gamma_c \geq \tau_c, \quad (5b)$$

$$\|\mathbf{w}\|^2 \leq P_t, \quad (5c)$$

$$|\Theta_{n,n}| = 1, \forall n = 1, \dots, N. \quad (5d)$$

The constraint (5b) imposes a lower bound threshold  $\tau_c$  on the user SNR, while constraint (5c) delineates the transmit power budget. Additionally, constraint (5d) enforces the unit-modulus constraint of the RIS. Various methodologies have been proposed to address the non-convex problem (5). However, these approaches often have elevated computational complexity stemming from iterative procedures or encounter performance degradation due to sub-optimal solutions.

### III. AN UNSUPERVISED LEARNING APPROACH TO BEAMFORMING DESIGN

In pursuit of simultaneously mitigating computational complexities and minimizing performance degradation, we introduce an unsupervised learning scheme for beamforming design in this section. Specifically, a closed-form expression for the transmit beamformer is provided first. Subsequently, we delve into the design of the unsupervised learning scheme for optimizing the RIS beamformer.

#### A. Transmit Beamforming Design

When RIS beamformer  $\Theta$  is determined, channels  $\mathbf{H}_t$  and  $\mathbf{h}_c^H$  are rendered constant. Consequently, the task becomes the optimization of the transmit beamformer, given as

$$\max_{\mathbf{w}} \|\mathbf{H}_t \mathbf{w}\|^2 \quad (6a)$$

$$s.t. \quad |\mathbf{h}_c^H \mathbf{w}|^2 \geq \tau_c \sigma_c^2, \quad \|\mathbf{w}\|^2 \leq P_t. \quad (6b)$$

A closed-form solution to problem (6) has been derived in [15], presented in the following theorem:

**Theorem 1.** *The optimal transmit beamformer  $\mathbf{w}$  is*

$$\mathbf{w} = \begin{cases} \sqrt{P_t} \frac{\mathbf{h}_t}{\|\mathbf{h}_t\|}, & \text{if } P_t |\mathbf{h}_c^H \mathbf{h}_t|^2 \geq \tau_c \sigma_c^2 \|\mathbf{h}_t\|^2; \\ x_1 \mathbf{u}_1 + x_2 \mathbf{u}_2, & \text{otherwise,} \end{cases} \quad (7)$$

where

$$\mathbf{u}_1 = \frac{\mathbf{h}_c}{\|\mathbf{h}_c\|}, \quad \mathbf{u}_2 = \frac{\mathbf{h}_t - (\mathbf{u}_1^H \mathbf{h}_t) \mathbf{u}_1}{\|\mathbf{h}_t - (\mathbf{u}_1^H \mathbf{h}_t) \mathbf{u}_1\|}, \quad (8)$$

and

$$\mathbf{x}_1 = \sqrt{\frac{\tau_c \sigma_c^2}{\|\mathbf{h}_c\|^2} \frac{\mathbf{u}_1^H \mathbf{h}_t}{|\mathbf{u}_1^H \mathbf{h}_t|}}, \quad \mathbf{x}_2 = \sqrt{P_t - \frac{\tau_c \sigma_c^2}{\|\mathbf{h}_c\|^2} \frac{\mathbf{u}_2^H \mathbf{h}_t}{|\mathbf{u}_2^H \mathbf{h}_t|}}. \quad (9)$$

Drawing from **Theorem 1**, a strong correlation between the two channels, given as  $|\mathbf{h}_c^H \mathbf{h}_t|^2$ , leads to a substantial overlap between the sensing and communication channel sub-spaces. As a result, even if the transmit beamformer aligns with the sensing channel, power can be effectively reused for communication, thus directly fulfilling the user SNR requirement. Conversely, when the correlation of the two channels is weak, the direct alignment beamformer falls short of satisfying the user SNR constraint. In such cases, the beamformer needs to be situated within the expanded subspace of  $\mathbf{h}_t$  and  $\mathbf{h}_c$  to maximize the echo SNR while concurrently meeting the communication SNR requirement.

#### B. RIS Beamforming Design

In this subsection, we introduce an unsupervised DL method for RIS beamformer design to enhance channel gain. This comprises three pivotal components: the generation of channel samples, the architecture of IBF-Net, and the formulation of an unsupervised loss function.

1) *Sample Constructions:* Our primary objective is to enhance the gains of the channels  $\mathbf{H}_t$  and  $\mathbf{h}_c$ . To achieve this, the samples are structured by extracting information from  $\mathbf{H}_t$  and  $\mathbf{h}_c$ . As discussed in Sec.II,  $\mathbf{H}_t$  and  $\mathbf{h}_c$  can be expressed as  $\mathbf{H}_t = \Phi_t^H \mathbf{v} \mathbf{v}^H \Phi_t$  and  $\mathbf{h}_c^H = \mathbf{v}^H \Phi_c$ . Consequently, the channel gains can be formulated as

$$\|\mathbf{H}_t\|^2 = \mathbf{v}^H \Phi_t \Phi_t^H \mathbf{v} \mathbf{v}^H \Phi_t \Phi_t^H \mathbf{v}, \quad (10a)$$

$$\|\mathbf{h}_c\|^2 = \mathbf{v}^H \Phi_c \Phi_c^H \mathbf{v}. \quad (10b)$$

Equation (10) illustrates that the channel characteristics are encapsulated within  $\Phi_t \Phi_t^H \in \mathbb{C}^{N \times N}$  and  $\Phi_c \Phi_c^H \in \mathbb{C}^{N \times N}$ , separated from the optimization variable  $\mathbf{v}$ . Therefore, we opt to utilize  $\Phi_t \Phi_t^H$  and  $\Phi_c \Phi_c^H$  for constructing the samples.

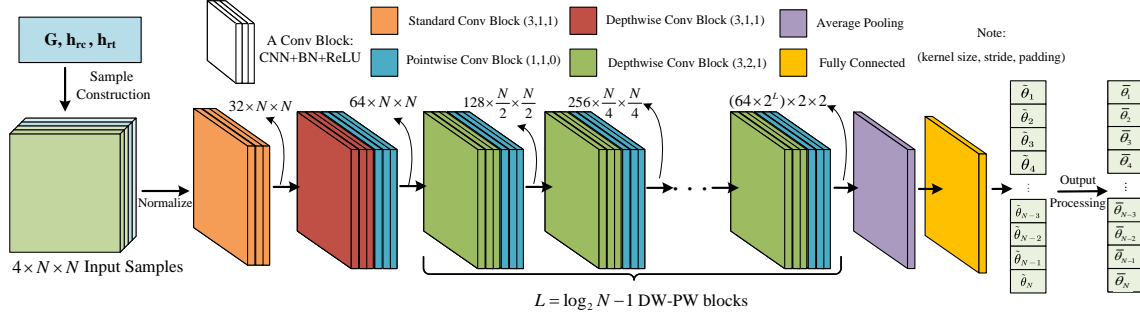


Fig. 1: Network Architecture of IBF-Net.

However, conventional neural networks are designed to process real numbers, whereas  $\bar{\Phi}_t \bar{\Phi}_t^H$  and  $\bar{\Phi}_c \bar{\Phi}_c^H$  are typically complex. Therefore, it is imperative to transform them into real representations. A straightforward approach is to extract the real and imaginary components, denoted as  $\mathcal{R}_t = \Re\{\bar{\Phi}_t \bar{\Phi}_t^H\}$ ,  $\mathcal{I}_t = \Im\{\bar{\Phi}_t \bar{\Phi}_t^H\}$ ,  $\mathcal{R}_c = \Re\{\bar{\Phi}_c \bar{\Phi}_c^H\}$ , and  $\mathcal{I}_c = \Im\{\bar{\Phi}_c \bar{\Phi}_c^H\}$ , respectively. Subsequently, we expand the dimensions of  $\mathcal{R}_t$ ,  $\mathcal{I}_t$ ,  $\mathcal{R}_c$ , and  $\mathcal{I}_c$  to  $\mathbb{R}^{1 \times N \times N}$  and concatenate them along the expanded dimension. Consequently, a constructed sample becomes a 3D tensor with dimensions of  $\mathbb{R}^{4 \times N \times N}$ .

2) *Network Architecture*: The architectural design of IBF-Net is illustrated in Fig. 1. Based on the performance efficacy and computational efficiency showcased in [10], we adopt a lightweight approach for the network components. This approach integrates structures of depthwise separable convolution (DW) and pointwise convolution (PW). Specifically, the network comprises a standard convolution block (Conv Block),  $L+1$  lightweight DW-PW Conv Blocks, and one fully connected layer. Each Conv Block consists of a Conv layer followed by a batch normalization (BN) layer and a rectified linear unit (ReLU) function. Prior to inputting the samples to IBF-Net, normalization is performed. Subsequently, a standard Conv Block is employed, where the Conv layer specifies the kernel size, stride, and padding as (3, 1, 1), yielding an output feature map size of  $32 \times N \times N$ . Following this,  $L+1$  DW-PW Conv Blocks are employed, where depthwise separable convolutions are performed with a kernel size of 3 and padding size of 1, while pointwise convolutions are executed in the PW blocks. The stride of the first DW block is set to 1 and the strides of the remaining  $L$  DW blocks are set to 2, thereby halving the feature map size and doubling its depth. Following the  $L$  DW-PW blocks, the output feature map dimension becomes  $(64 \times 2^L) \times 2 \times 2$ . Then, an average pooling layer of size 2 and a fully connected layer are employed to predict  $\hat{\theta}$ .

However, the network output  $\hat{\theta}$  does not inherently satisfy the constraint (5d). Therefore, post-processing is necessary to ensure adherence to the unit-modulus constraint. Specifically, we apply the Euler formula [10] to  $\hat{\theta}$ , resulting in the expression of

$$\bar{\theta} = \cos \tilde{\theta} + j \sin \tilde{\theta}. \quad (11)$$

Consequently, following this post-processing step, the final output  $\bar{\theta}$  represents the designed RIS phases, satisfying the constraint (5d).

3) *Loss Design*: In the training phase, it is crucial to design an effective loss function to facilitate the update of network parameters. Traditional optimization methods for RIS

beamformer design through manual labeling are notably time-consuming. To circumvent extensive labeling efforts, an unsupervised learning mechanism is employed to formulate the loss function, thereby promoting training for enhancing both sensing and communication channel gains.

Inspired by [6], the presence of RIS introduces additional channels, effectively expanding the sensing and communication channel subspaces. Through adjustment of phase shifts, RIS can manipulate the orientation of the subspaces, thereby enhancing their correlations. As elucidated in Sec.III-A, increasing correlation of the two channels facilitates power reuse, which enhances both channel gains. Consequently, the network is trained to manipulate RIS phase shifts to increase correlation of the two channels. This gives a loss function as

$$l_1 = -\frac{1}{S} \sum_{s=1}^S \|\mathbf{H}_t^s \mathbf{h}_c^s\|_2, \quad (12)$$

in which  $S$  denotes the mini-batch size (mbs) during training phase. As the loss function  $l_1$  decreases, it indicates an increase in the correlations of the two channels, leading to the concurrent enhancement of both channel gains.

However, relying solely on  $l_1$  as a loss function may yield results that the communication channel gain significantly surpasses the sensing channel gain, as will be demonstrated in Sec.IV. This discrepancy arises from the fact that the sensing channel is subject to double fading in bidirectional propagation, while the communication channel experiences fading only once. Consequently, unless the user SNR threshold is sufficiently high, the communication SNR may substantially exceed the preset threshold, while the radar SNR suffers from performance degradation compared to numerical optimization outcomes. To address this challenge, we introduce the sensing channel gain in the loss function, aiming to balance the correlation of the two channels and the sensing channel gain. This is mathematically expressed as:

$$l_2 = -\frac{1}{S} \sum_{s=1}^S (\|\mathbf{H}_t^s \mathbf{h}_c^s\|_2 + \alpha \|\mathbf{H}_t^s\|_F), \quad (13)$$

where  $\alpha$  represents a balancing coefficient employed to trade off the sensing channel gain and the correlation between the two channels. Different  $\alpha$  leads to different training results, where a well-selected  $\alpha$  balances the sensing and communication performance while excessively small or large  $\alpha$  results in performance bias thereby reducing performance. The effect of varying  $\alpha$  will be demonstrated in Sec.IV. Specifically,  $l_1$  corresponds to a special case of  $l_2$  when  $\alpha$  is set to 0.

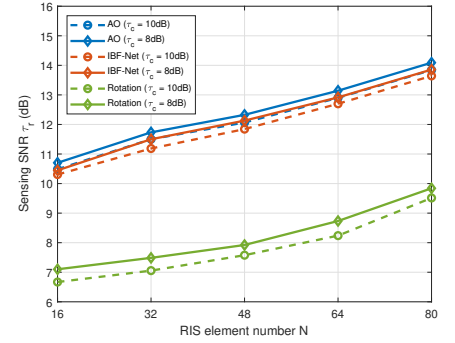
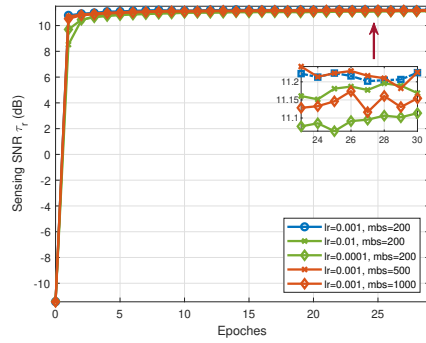
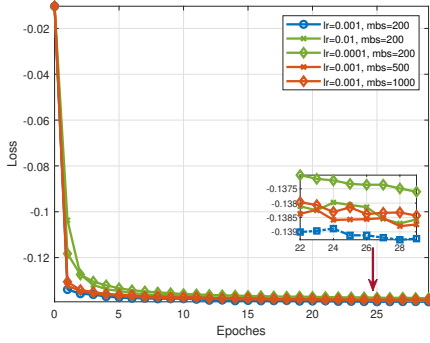


Fig. 2: Changes of losses during training. Fig. 3: Changes of  $\tau_r$  during training. Fig. 4: RIS element number effect on  $\tau_r$ .

### C. Overall Algorithm

In training phase, an extensive set of channel measurements are gathered to construct samples, as shown in Sec.III-B1. Then, IBF-Net is trained with  $l_2$  loss function. In testing phase, samples are constructed and input to the well-trained network. After obtaining RIS beamformer from the network, the overall channels  $\mathbf{h}_t$  and  $\mathbf{h}_c$  are computed. Subsequently, the transmit beamforming is obtained by using **Theorem 1**.

## IV. SIMULATION RESULTS

In this section, simulations are conducted, where we first outline the model configurations, hardware settings and comparison benchmarks. Then, we present experiments on the variations of loss and objectives in training, the impact of different coefficients, and the computational complexities.

### A. Simulation Settings

Unless stated otherwise, the BS is equipped with 8 antennas, and the RIS comprises 32 elements. Additionally, the transmit power is restricted to  $P=8$  dBm, while the noise power is set to  $\sigma_r^2=\sigma_c^2=-20$  dBm. The user SNR threshold  $\tau_c$  is established at 10 dB. All channels are characterized as Rician channels [10], with Rician factors set to 10. For training purposes, the IBF-Net is implemented with PyTorch framework, trained on an NVIDIA Tesla P40 GPU. We generate 500,000 samples to train the model, with training mbs and learning rate (lr) set to 200 and 0.001, unless specific specifications. Additionally, the balancing coefficient  $\alpha$  is set to 0.8. During the training process, we utilize Adam optimizer to update network parameters for 30 epochs. For testing purposes, 100 samples are used to evaluate the generalization capability of the model.

To evaluate the proposed method, we compare it against two representative algorithms. The first benchmark, described in [3], alternately optimizes active and passive beamformers with MM and SDR, yielding near-optimal solutions. Conversely, the subspace rotation approach proposed in [6] serves as the second baseline, featuring rapid designs for RIS and transmit beamformers through non-alternative dual-variable optimization. For ease of expression, we denote the first benchmark as “AO” and abbreviate the second baseline as “Rotation”.

### B. Performance Evaluations

We first show the evolution of loss during the training phase in Fig. 2. The network undergoes training across various combinations of lr and training mbs, where the lr ranges from 0.01 to 0.0001, and mbs is set to 200, 500, and 1000, respectively. Evidently, all settings exhibit convergence, albeit with slight discrepancies in the convergence trajectories attributed to different parameter combinations. Notably, cases with lr=0.001 demonstrate faster initial decreases in loss, converging to lower levels compared to other cases. Conversely, scenarios with lr=0.01 initially converge slowly but eventually surpass those with lr=0.0001, owing to their larger step sizes. Meanwhile, cases with lr=0.0001 continue reducing in loss beyond 30 epochs. Furthermore, observations across different mbs reveal a marginal enhancement in convergence with smaller mbs.

The variations in the average sensing SNR ( $\tau_r$ ) of the testing samples during the training phase are illustrated in Fig. 3. These results are documented under the same settings used in the previous experiment. It is evident that the average sensing SNRs show a consistent increase throughout the training process across all cases, affirming the efficacy of the proposed method. Moreover, by comparing the  $\tau_r$  under different settings, it is notable that evolution trend of  $\tau_r$  is closely related to the changes of loss.

Fig. 4 shows the impact of RIS element number on sensing SNR, alongside comparisons with benchmarks. As the element number ( $N$ ) increases, the sensing SNRs of all approaches rise, which aligns with intuitive expectations as more elements provide greater degrees of freedom. Furthermore, the proposed scheme demonstrates significantly closer performance to the “AO” scheme than the “Rotation” scheme. This is attributed to the neural network’s ability to handle high-dimensional and non-convex problems, facilitating avoidance from local optima. Additionally, an inverse relationship is observed between the sensing SNR ( $\gamma_r$ ) and the user SNR threshold ( $\tau_c$ ) as  $\tau_c$  increases. This phenomenon underscores the spectrum resource tradeoff between sensing and communication.

To assess the impact of the balancing coefficient  $\alpha$ , IBF-Net is trained using varying  $\alpha$  under different configurations, and the results are shown in Table I. Observations reveal that as  $\alpha$  ranges from 0 to 1.6, the sensing SNR ( $\gamma_r$ ) gradually increases while the communication SNR ( $\gamma_c$ ) decreases, getting closer to the user SNR threshold ( $\tau_c$ ). This stems from the fact

TABLE I: Sensing SNR  $\gamma_r$  and Communication SNR  $\gamma_c$  under different balancing factor  $\alpha$ 

Different Settings	$\gamma_r$ & $\gamma_c$ (dB)	Varing $\alpha$							
		-0.8	-0.4	0	0.4	0.8	1.6	3.2	4.8
$\tau_c = 10\text{dB}$ , $P = 8\text{dBm}$	Sensing SNR $\gamma_r$	-19.96	-0.25	8.72	10.74	11.22	11.3	10.93	10.77
	Comm. SNR $\gamma_c$	9.89	11.69	17.38	12.82	10.59	10.18	10.01	9.98
$\tau_c = 8\text{dB}$ , $P = 8\text{dBm}$	Sensing SNR $\gamma_r$	-21.19	-0.16	8.90	10.89	11.31	11.52	11.45	11.37
	Comm. SNR $\gamma_c$	8.08	21.10	17.25	13.58	10.71	9.08	8.46	8.26
$\tau_c = 8\text{dB}$ , $P = 10\text{dBm}$	Sensing SNR $\gamma_r$	-19.55	1.54	10.76	12.77	13.27	13.48	13.41	13.37
	Comm. SNR $\gamma_c$	10	23.07	19.4	15.11	11.95	10.5	10.34	10.11

that  $\alpha$  effectively balancing the gains of the sensing channel and the correlation between the channels to facilitate resource allocation. Specifically, when  $\alpha=0$  (i.e.  $l_1$  is considered), the  $\gamma_c$  significantly exceeds the preset threshold  $\tau_c$  at the cost of reducing  $\gamma_r$ . As  $\alpha$  continues to increase,  $\gamma_r$  experiences slight degradation while  $\gamma_c$  progressively fails to meet the constraint. This attributes to the predominant allocation of energy to sensing, leading to degradation of communication SNR. Meanwhile, the transmit beamformer endeavors to satisfy the user SNR constraint, allocating fewer resources to sensing, resulting in a marginal decrease in  $\gamma_r$ . Conversely, when  $\alpha$  is less than zero, both  $\gamma_r$  and  $\gamma_c$  exhibit sharp declines, as negative  $\alpha$  adversely affects the sensing channel, diminishing the correlation of the two channels. Furthermore, it is noted that as transmit power increases or communication constraints relax, the permissible range of  $\alpha$  widens. This implies the importance of selecting  $\alpha$ , as excessively large or small values may yield unfavorable outcomes.

### C. Complexity Comparisons

To evaluate computational complexities, we compare the running times of the proposed method to those of benchmarks in Table II. The running time is computed as the average duration for designing the system beamformers with 100 channel realizations. The results in Table II show that the proposed method consumes the least time compared to the benchmarks. Specifically, the "AO" approach consumes nearly 1000 times more computational resources than the proposed method. Additionally, the time complexity of the "Rotation" scheme is marginally higher than that of the proposed method. This difference arises from the gradient descent utilized by the "Rotation" scheme, which entails an iterative search process. In summary, the proposed method achieves high performance while significantly reduces computational resources, thus demonstrating its efficiency and effectiveness.

TABLE II: Average running time of one sample (ms)

Time	Algorithm	AO	LRCNN	Rotation
Parameters				
	N = 16	$3.63 \times 10^3$	3.7	4.2
	N = 32	$6.61 \times 10^3$	3.9	5.4
	N = 48	$13.65 \times 10^3$	4.1	11.0
	N = 64	$22.71 \times 10^3$	4.6	16.3
	N = 80	$37.76 \times 10^3$	5.2	20.2

## V. CONCLUSIONS

This paper introduced an unsupervised learning method for beamforming design in a RIS-aided ISAC system. Specifically, an IBF-Net model was developed for RIS beamforming,

leveraging image-shaped channel samples. Moreover, we formulated a loss function to balance the sensing and communication channel correlations, as well as sensing channel gain. Subsequently, the transmit beamformer was obtained by a closed-form expression. Simulations showed that our proposed unsupervised learning-based beamforming method yielded satisfying performance and substantially reduced computational complexities.

## REFERENCES

- [1] Z. Chen, G. Chen, J. Tang, S. Zhang, D. K. So, O. A. Dobre, K.-K. Wong, and J. Chambers, "Reconfigurable intelligent-surface-assisted B5G/6G wireless communications: Challenges, solution, and future opportunities," *IEEE Commun. Mag.*, vol. 61, no. 1, pp. 16–22, 2023.
- [2] M. Rihan, A. Zappone, and S. Buzzi, "Robust RIS-assisted MIMO communication-radar coexistence: Joint beamforming and waveform design," *IEEE Trans. Commun.*, vol. 71, no. 11, pp. 6647–6661, 2023.
- [3] Z.-M. Jiang, M. Rihan, P. Zhang, L. Huang, Q. Deng, J. Zhang, and E. M. Mohamed, "Intelligent reflecting surface aided dual-function radar and communication system," *IEEE Syst. J.*, vol. 16, no. 1, pp. 475–486, 2022.
- [4] S. Yan, S. Cai, W. Xia, J. Zhang, and S. Xia, "A reconfigurable intelligent surface aided dual-function radar and communication system," in *IEEE Int. Symp. Jt. Commun. Sens., JC and S*, 2022, pp. 1–6.
- [5] R. Liu, M. Li, Y. Liu, Q. Wu, and Q. Liu, "Joint transmit waveform and passive beamforming design for RIS-aided DFRC systems," *IEEE J. Sel. Top. Signal Process.*, vol. 16, no. 5, pp. 995–1010, 2022.
- [6] X. Meng, F. Liu, S. Lu, S. P. Chepuri, and C. Masouros, "RIS-assisted integrated sensing and communications: a subspace rotation approach: invited paper," in *Proc. IEEE Radar. Conf.*, 2023, pp. 1–6.
- [7] C. Huang, G. C. Alexandropoulos, C. Yuen, and M. Debbah, "Indoor signal focusing with deep learning designed reconfigurable intelligent surfaces," in *Proc. IEEE 20th Int. Workshop Signal Process. Adv. Wireless Commun.*, 2019, pp. 1–5.
- [8] J. Gao, C. Zhong, X. Chen, H. Lin, and Z. Zhang, "Unsupervised learning for passive beamforming," *IEEE Commun. Lett.*, vol. 24, no. 5, pp. 1052–1056, 2020.
- [9] Y. Ge and J. Fan, "Beamforming optimization for intelligent reflecting surface assisted MISO: a deep transfer learning approach," *IEEE Trans. Veh. Technol.*, vol. 70, no. 4, pp. 3902–3907, 2021.
- [10] Z. Chen, J. Ye, P. Zhang, H. Rizk, L. Huang, and M. Rihan, "A light-weight learning framework for RIS-assisted beamforming design with mobile edge computing," in *IEEE/CIC Int. Conf. Commun. China*, 2023, pp. 1–6.
- [11] K. Feng, Q. Wang, X. Li, and C.-K. Wen, "Deep reinforcement learning based intelligent reflecting surface optimization for MISO communication systems," *IEEE Wireless Commun. Lett.*, vol. 9, no. 5, pp. 745–749, 2020.
- [12] J. Mu, Y. Gong, F. Zhang, Y. Cui, F. Zheng, and X. Jing, "Integrated sensing and communication-enabled predictive beamforming with deep learning in vehicular networks," *IEEE Commun. Lett.*, vol. 25, no. 10, pp. 3301–3304, 2021.
- [13] X. Liu, H. Zhang, K. Long, A. Nallanathan, and V. C. M. Leung, "Distributed unsupervised learning for interference management in integrated sensing and communication systems," *IEEE Trans. Wireless Commun.*, vol. 22, no. 12, pp. 9301–9312, 2023.
- [14] A. M. Ahmed, L. Gharsalli, S. Fortunati, and A. Sezgin, "Reinforcement learning for cognitive integrated communication and sensing systems," in *European Radar Conf.*, 2023, pp. 395–398.
- [15] F. Liu, Y.-F. Liu, A. Li, C. Masouros, and Y. C. Eldar, "Cramér-Rao bound optimization for joint radar-communication beamforming," *IEEE Trans. Signal Process.*, vol. 70, pp. 240–253, 2022.